**Equivalent: Jurnal Ilmiah Sosial Teknik**
**Volume 8, Issue 5, 2364-2385**
**e_ISSN: 2775-0833**
https://jurnalequivalent.id/index.php/jequi/index
DOI: doi.org/10.59261/jequi.v8i5.490

# Comparative Analysis of Thermodynamic Performance and Emissions of Natural Gas and Ammonia as Fuels for an H Class Gas Turbine

**Dapot Bonitua Rajagukguk***
Universitas Diponegoro, Indonesia

**S. Silviana**
Universitas Diponegoro, Indonesia

**M. Muchammad**
Universitas Diponegoro, Indonesia

***Corresponding author:**
Dapot Bonitua Rajagukguk, Universitas Diponegoro, Indonesia.
✉bona1218@students.undip.ac.id

**Article Info:**
***Article history:***
Received: September 30, 2026
Revised: October 28, 2026
Accepted: October 30, 2026
Available Online: November 09, 2026

***Keywords:***
Ammonia;
Carbon Dioxide Emissions;
H Class Gas Turbine;
Natural Gas;
Nitric Oxide Emissions;
Thermodynamic Performance;

This is an open access article under the CC BY-SA license.

Copyright © 2026 by Author. Published by Politeknik Siber Cerdika International

**Abstract**

**Background:** Ammonia is a carbon-free fuel candidate, but its performance in utility-scale H-class gas turbines requires assessment under representative plant operating conditions.
**Objective:** To compare the performance of natural gas and ammonia, their respective fuel requirements, and their predicted equilibrium emissions in a GE 9HA.02 gas turbine at PLTGU Cilamaya.
**Methods:** A steady-state model was developed in DWSIM using the Peng–Robinson property package and a Gibbs reactor and was evaluated at five load conditions derived from distributed control system (DCS) data. Simulations at equal fuel mass flow rates were compared, and inverse regression was used to estimate the ammonia mass flow rates required to achieve equivalent net power output.
**Results:** Net power output ranged from 199.227 to 592.771 MW for natural gas, compared with 70.455–228.870 MW for ammonia at equal fuel mass flow rates. Ammonia provided 37.58% of the natural gas heat input and retained 32.28–38.61% of its net power output. Thermal efficiency ranged from 28.85% to 49.96% for natural gas and from 27.15% to 51.33% for ammonia. Inverse regression estimated ammonia mass flow rates of 22.214–47.093 kg/s; these estimates require load-specific verification. The model predicted zero direct $CO_2$ emissions from pure ammonia and a 94.91–96.36% reduction in equilibrium NO mass flow rate. A weighted performance index favored Load III among the modeled conditions.
**Conclusion:** Ammonia substitution requires higher fuel mass flow rates and further assessment of combustion behavior and equipment constraints. The available calibration evidence does not establish independent model validation. Equilibrium NO predictions and extrapolated estimates of ammonia requirements for equivalent net power output are insufficient to establish full-scale operating feasibility.

**To cite this article:** Rajagukguk, D. B., Silviana, S., & Muchammad, M. (2026). Comparative analysis of thermodynamic performance and emissions of natural gas and ammonia as fuels for an H class gas turbine. *Equivalent: Jurnal Ilmiah Sosial Teknik, 8*(5), 2364-2385. https://doi.org/10.59261/jequi.v8i5.490

## INTRODUCTION

Global efforts toward low-carbon energy systems have increased interest in alternative fuels for power generation. Kang et al. (2023) identify ammonia blending as a relevant pathway for industrial combustion applications. Fossil-fuel-based power generation remains an important target for decarbonization (Valera-Medina et al., 2018). Ammonia ($NH_3$) is a carbon-free fuel because its molecular structure contains no carbon; consequently, the combustion of pure ammonia produces no fuel-derived $CO_2$. Ammonia can be synthesized using renewable hydrogen and nitrogen separated from the atmosphere, although its life-cycle emissions depend on the production and supply pathways employed. Saif & Mokheimer (2025) discuss its potential as a hydrogen carrier and energy

vector. Nevertheless, ammonia's low reactivity, narrow flammability limits, slow flame propagation, and potential for nitrogen oxide formation complicate its use in industrial combustion systems. Pashchenko (2023) emphasizes that ammonia combustion requires combustor modifications relative to those used for conventional fuels.

Previous studies have investigated ammonia combustion in gas turbines through experiments and thermodynamic cycle modeling. Kurata et al. (2017) demonstrated power generation in a 50-kW micro gas turbine using $NH_3$–air and $NH_3$–$CH_4$–air combustion. Okafor et al. (2019) investigated staged combustion to reduce $NO_x$ emissions, whereas Somarathne et al. (2017) examined secondary air injection under elevated-pressure conditions. Saif & Mokheimer (2025) reviewed the effects of fuel blending and combustor configuration on emissions. Xiao et al. (2017) investigated the combustion characteristics of premixed ammonia–methane mixtures. At the thermodynamic cycle level, Keller et al. (2020) evaluated an ammonia-fueled, fuel-rich combined-cycle process, while Guteša Božo et al. (2019) investigated ammonia–hydrogen injection in humidified gas turbines. Fawwaz Aalrebei et al. (2022) analyzed ammonia–hydrogen–air cycles and their control strategies. Pashchenko (2024) reviewed progress toward larger ammonia-fired gas turbines, including the H-25 development program. L. Liu et al. (2022) extended the discussion to ammonia–diesel stratified injection for marine applications.

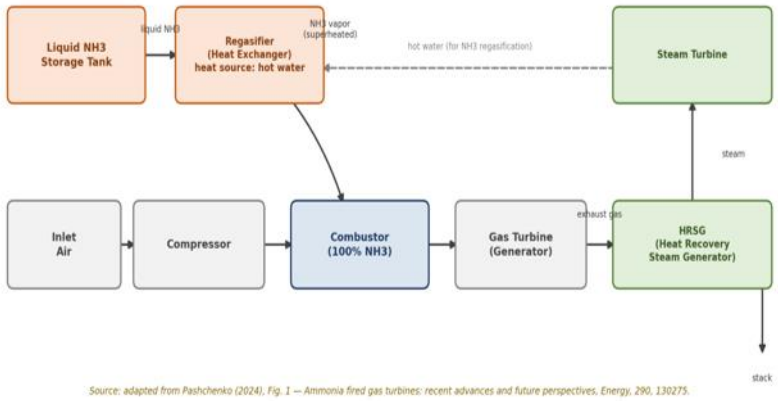



**Figure 1**. Schematic of an ammonia-fueled H-25 gas turbine with a heat recovery steam generator and steam turbine. Adapted from (Pashchenko, 2024).

Most published evidence on ammonia-fueled gas turbines concerns laboratory-scale combustors, micro gas turbines, or thermodynamic cycle models. Kurata et al. (2017) demonstrated micro gas turbine operation, whereas Keller et al. (2020) evaluated a thermodynamic combined-cycle process. However, these studies do not establish the performance of ammonia combustion in an operating utility-scale H-class gas turbine. The present study uses DWSIM to model a GE 9HA.02 gas turbine under five operating conditions derived from Distributed Control System (DCS) data. Hassan & Manji (2023) provide a precedent for DWSIM-based power plant performance assessment. The model compares fuel heat input, combustion and exhaust temperatures, compressor and turbine work, net power output, thermal efficiency, and equilibrium-predicted $CO_2$ and NO concentrations for natural gas and ammonia. Plant data are used to constrain the natural gas baseline but do not independently validate the modeled ammonia combustion performance or emissions.

To address the limited evidence regarding ammonia substitution in utility-scale H-class gas turbines, this study investigates three research objectives. First, it compares the thermodynamic performance of natural gas and ammonia at equal fuel mass flow rates under five operating conditions derived from the Distributed Control System (DCS) data of PLTGU Cilamaya. The comparison includes heat input, combustion and exhaust temperatures, compressor and turbine work, net power output, and thermal efficiency (RQ1). Second, it estimates the ammonia mass flow rate required to match the simulated net power output of natural gas and examines variations in fuel requirements and performance differences across operating loads (RQ2). Third, it evaluates the relationship between thermodynamic performance and equilibrium-predicted

carbon dioxide ($CO_2$) and nitric oxide (NO) emissions to identify the most favorable operating condition according to the selected evaluation criteria (RQ3). By integrating plant-derived operating conditions with DWSIM simulations, this study provides a comparative thermodynamic assessment of ammonia substitution while acknowledging the limitations of equilibrium combustion modeling and the absence of independently validated operating data for ammonia-fueled H-class gas turbines.

## METHOD

Figure 2 presents the framework used to evaluate natural gas and ammonia as fuels for an H-class gas turbine under five actual load conditions. The study was designed around objectives related to thermodynamic performance, fuel demand, and emission formation. Primary data obtained from the Distributed Control System (DCS) included compressor air flow, temperatures, pressures, fuel flow, exhaust conditions, and net load. Journal articles, energy roadmaps, and thermodynamic data provided fuel properties, modeling assumptions, and evidence from previous studies. Together, these sources established the operating boundaries for a representative steady-state model.

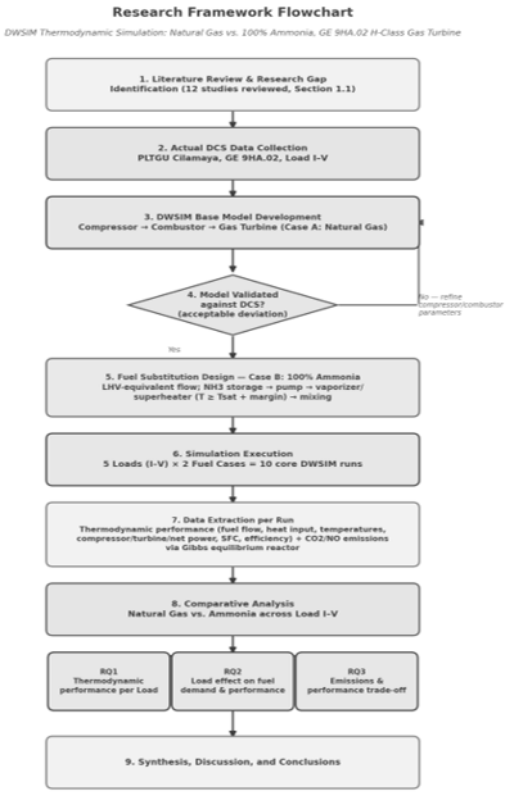



**Figure 2.** Research framework for the comparative simulation of natural gas and ammonia fuels

The compressor, Gibbs reactor, and turbine were modeled using the Peng–Robinson property package. Calibration was defined as the adjustment of model parameters against plant data, whereas validation was defined as the evaluation of predictions against independent data not used for adjustment. The five DCS load points defined the operating boundary conditions and permitted an in-sample baseline assessment, but not independent validation. The simulated net power outputs for natural gas were 199.227, 309.623, 375.413, 427.819, and 592.771 MW, compared with DCS-recorded loads of 249.651, 300.564, 351.438, 400.038, and 500.303 MW. Thus, only Load II satisfied the 5% net power deviation criterion. The comparisons at the other loads remained exploratory.

Following the baseline assessment, natural gas and ammonia simulations were compared under the five DCS-derived air-flow and pressure conditions. The reported RQ1 results were based on equal fuel mass flow rates; net power output was not held constant. The comparison included heat input, temperatures, compressor and turbine work, net power output, thermal

efficiency, $CO_2$, and NO. Separate heat-equivalence calculations and inverse-regression estimates were used to examine alternative fuel-substitution bases. Neither calculation established a feasible operating point at equal net power without additional simulations under fixed boundary conditions.

**Gas Turbine**

The research subject was an H-class gas turbine in an Indonesian combined-cycle power plant. A gas turbine converts the chemical energy of fuel into shaft work through the Brayton cycle, which involves compression, heat addition, and expansion. Figure 3 illustrates two gas turbine configurations: (a) a simple-cycle gas turbine (open cycle) and (b) a closed-cycle gas turbine (Çengel, 2004). In the open cycle, ambient air is compressed before entering the combustion chamber. Fuel combustion produces hot gases that expand through the turbine. Part of the turbine work drives the compressor, while the remaining shaft work drives the generator. In combined-cycle operation, exhaust heat can be recovered in a heat recovery steam generator (HRSG) to produce additional power (GE Vernova, 2020).

The H-class gas turbine was selected because it represents an advanced heavy-duty gas turbine characterized by a high pressure ratio, elevated turbine inlet temperature, high power output, and flexible response to load variations. Under standard reference conditions, the 9HA.02 gas turbine has a nominal simple-cycle net output of approximately 571 MW and a net thermal efficiency of approximately 44% based on the lower heating value (LHV). When integrated into a single-shaft combined-cycle configuration, its nominal output can reach approximately 838 MW, with a net thermal efficiency of approximately 64.1%. These reference ratings depend on ambient conditions, fuel composition, plant configuration, auxiliary consumption, and operating strategy. Actual plant performance may therefore differ from published design values.

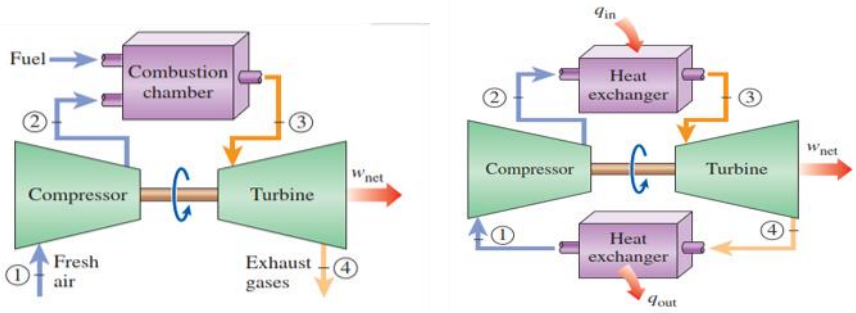



**Figure 3.** (a) Simple-cycle gas turbine; (b) closed-cycle gas turbine.

**Gas Turbine Thermodynamic cycle**

The thermodynamic cycle underlying the gas turbine described above is the Brayton cycle (Figure 4). In its idealized form, the cycle comprises isentropic compression (1–2), constant-pressure heat addition (2–3), isentropic expansion (3–4), and heat rejection (4–1). In an actual open-cycle gas turbine, however, the exhaust gases are discharged into the atmosphere rather than returned to the compressor inlet. Figure 4 presents the cycle on a temperature–entropy (T–s) diagram, plotted using the representative state-point data reported by Keller et al. (2020) for a combined-cycle model with an equivalence ratio of 1.2, an exhaust gas recirculation ratio of 0.4, and a pressure ratio of 20, as specified in their Table 1. Ambient air enters the compressor at State 1 (298.15 K, 1 bar) and leaves at State 2 (757.08 K, 20 bar). Heat addition in the combustor then raises the gas temperature to the turbine inlet temperature at State 3 (2010.98 K, 20 bar). Expansion through the turbine subsequently brings the gas to State 4 (1225.30 K, 1 bar) before exhaust. Table 1 reproduces these state points (Keller et al., 2020).

Two features of Figure 4 warrant discussion. First, the modest rightward entropy shifts during compression (1–2) and expansion (3–4), rather than perfectly vertical isentropic lines, reflect the nonunity isentropic efficiencies ($\eta c = 0.85$, $\eta t = 0.80$) used by Keller et al. (2020) to represent irreversibilities in the actual compressor and turbine. An idealized cycle with $\eta c = \eta t = 1$ would instead exhibit vertical lines at constant entropy. Second, the substantially larger entropy increase during combustion (2–3) reflects both the heat released by fuel oxidation and the

chemical contribution to entropy associated with changes in the working fluid's composition. A treatment based solely on sensible heat would omit this chemical contribution. Accordingly, Keller et al. (2020) calculated the State 3 conditions through Gibbs free-energy minimization rather than by applying a simple constant-pressure temperature rise.

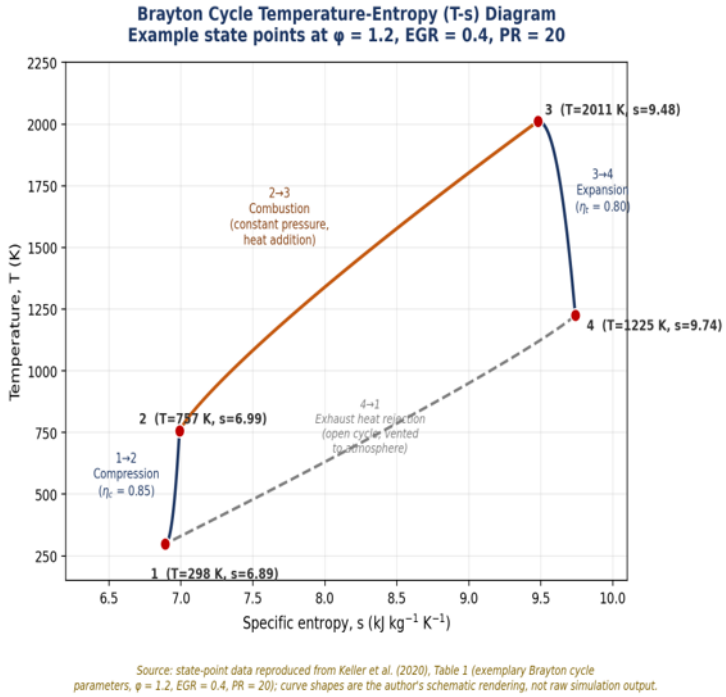



**Figure 4.** Temperature–entropy (T-s) diagram of the Brayton cycle, plotted from (Keller et al., 2020)

**Table 1**

*Temperature–entropy (T-s) diagram of the Brayton cycle, plotted from (Keller et al., 2020)*

| State | Description | Temperature, T (K) | Pressure, P (bar) | Entropy, s (kJ kg$^{-1}$ K$^{-1}$) |
|---|---|---|---|---|
| 1 | Compressor inlet (ambient air) | 298.15 | 1 | 6.89 |
| 2 | Compressor outlet | 757.08 | 20 | 6.99 |
| 3 | Turbine inlet (TIT, after combustion) | 2010.98 | 20 | 9.48 |
| 4 | Turbine outlet / exhaust | 1225.30 | 1 | 9.74 |

**Gas Turbine Fuel**

Fuel selection for gas turbines has changed considerably since the technology's industrial adoption during the previous century. Early heavy-duty and aeroderivative units commonly used liquid distillate or kerosene-type fuels because pipeline gas infrastructure was not yet widespread. Natural gas gradually displaced these liquid fuels as pipeline networks expanded and combined-cycle configurations made gas-fired power increasingly cost-competitive. Consequently, most existing utility-scale gas turbine plants, including the 9HA.02 unit examined in this study, use natural gas as their primary fuel (Pashchenko, 2023).

Ammonia's potential as a gas turbine fuel predates its recent prominence in the decarbonization literature. Early combustion studies conducted more than half a century ago demonstrated that ammonia could sustain combustion in gas turbine burners and combustors (Keller et al., 2020). However, the availability of inexpensive and abundant natural gas left these early findings largely dormant for decades. Renewed interest in carbon-free power generation subsequently revived ammonia combustion research from the mid-2010s onward. Initial developments focused on micro gas turbines Kurata et al. (2014), followed by developments at larger scales. Examples included Turboden's 15-MW ammonia-capable cogeneration unit installed in Germany in 2018, Mitsubishi Power's 2020 announcement of a 40-MW H-25-based

turbine designed for 100% ammonia firing, and additional units under development at MAN Energy Solutions and Kawasaki Heavy Industries (Pashchenko, 2024).

**Table 2**
*Thermal properties of ammonia and methane (natural gas reference)*

| Property | Ammonia ($NH_3$) | Methane ($CH_4$, natural gas reference) |
|---|---|---|
| Boiling temperature at 1 atm (°C) | −33.4 | −161 |
| Lower heating value, LHV (MJ/kg) | 18.6 | 50.0 |
| Flammability limit (equivalence ratio, φ) | 0.63–1.40 | 0.50–1.7 |
| Adiabatic flame temperature (°C) | 1800 | 1950 |
| Maximum laminar burning velocity (m/s) | 0.07 | 0.37 |
| Minimum autoignition temperature (°C) | 650 | 630 |

Table 2 presents the principal thermal properties of ammonia and methane as reference fuels. The reported lower heating values were 18.6 MJ/kg for ammonia and 50.0 MJ/kg for methane (Kobayashi et al., 2019). Because natural gas composition varies, the heating value of pure methane should not be interpreted as the measured heating value of the natural gas supplied to PLTGU Cilamaya. Based on the reported fuel mass flow rates and energy inputs, the simulation calculations implied an effective natural gas LHV of approximately 49.5 MJ/kg. This value was therefore used consistently as the energy-accounting basis for the simulations, although its correspondence with the actual plant fuel composition requires confirmation from the original fuel-property records.

At equal fuel mass flow rates, ammonia provided approximately 37.58% of the simulated natural gas heat input, corresponding to an energy reduction of 62.42%. Based on the respective LHV values of 49.5 and 18.6 MJ/kg, achieving equal heat input required approximately 2.661 times the natural gas mass flow rate when ammonia was used. The corresponding ammonia flow estimates are presented in Table 3. These calculations established energy equivalence only and did not demonstrate equivalent gas turbine net power output, combustion stability, or operational feasibility.

**DWSIM Software**

The thermodynamic model developed for this study was constructed entirely in DWSIM, a free, open-source chemical process simulator that provides a graphical, steady-state flowsheet environment comparable to commercial packages such as Aspen HYSYS, Aspen Plus, and GateCycle. Hassan & Manji (2023), whose comparative study of DWSIM and Aspen HYSYS motivated its selection for this study, described the platform's library of unit operations, including compressors, turbines, heat exchangers, mixers, valves, pumps, and reactors. They also described its selection of thermodynamic property packages, including the Peng–Robinson and Soave–Redlich–Kwong cubic equations of state, which users can assemble into a flowsheet representing the physical process being modeled.

The suitability of DWSIM for this study was assessed in light of the precedent reported by (Hassan & Manji, 2023). When benchmarked directly against Aspen HYSYS using an identical combined-cycle configuration, DWSIM predicted essentially the same power output, while the difference in thermal efficiency was approximately 3.5%. More importantly, when calibrated against actual operating data from a commercially operating combined-cycle gas turbine plant, DWSIM reportedly reproduced net power output with a deviation of approximately 0.45%. For a cogeneration configuration incorporating an HRSG, deviations across several turbine and net-power parameters ranged from 0.26% to 4.79%. These results were obtained for natural-gas-fired systems rather than ammonia-fired systems. They supported the selection of DWSIM for assessing the 9HA.02 natural gas baseline against actual DCS data in Section 2.4. However, the larger net power deviations obtained in the present baseline assessment (−20.20% to +18.48%) were reported transparently as a limitation of the model developed in this study, rather than as a limitation of DWSIM itself.

Within DWSIM, the base model corresponded to the Brayton-cycle states introduced in the

preceding section. A Compressor unit operation represented compression from State 1 to State 2, a Combustion Chamber configured as a Gibbs free-energy equilibrium reactor represented heat addition from State 2 to State 3, and a Gas Turbine unit operation represented expansion from State 3 to State 4. These components were configured consistently with the governing equations attributed to Keller et al. (2020) in the preceding sections. Case B additionally incorporated an $NH_3$ Storage stream, an $NH_3$ Pump, and an $NH_3$ Vaporizer/Superheater upstream of the fuel-mixing unit to represent the ammonia-conditioning train described earlier. Figure 6 illustrates the two fuel paths as configured in the DWSIM flowsheet.

The Peng–Robinson or Soave–Redlich–Kwong cubic equation of state was applied in the simulations, with the limitations of these models for ammonia vapor–liquid equilibrium taken into account. Ammonia's strongly polar, self-associating molecular structure can reduce the accuracy of these equations of state near its critical point (132.4 °C, 113.5 bar). This limitation, discussed further in the subsequent section, informed the design of the ammonia vaporizer/superheater in Case B. The unit was intended to produce fully superheated ammonia vapor sufficiently far from the saturation curve before the fuel stream was mixed and modeled, rather than relying on the property package to resolve a near-critical, two-phase ammonia stream accurately.

Combustion in both cases was modeled using DWSIM's Gibbs reactor, which determines equilibrium product composition and, consequently, combustion gas temperature by minimizing Gibbs free energy over a specified set of chemical species rather than by solving detailed reaction kinetics. Keller et al. (2020) used the same computational approach to determine the turbine inlet temperature discussed in Section 5.1. This approach is suitable for estimating major combustion products and $CO_2$ formation from mass and energy balances, subject to the assumptions of equilibrium modeling. However, Hassan et al. (2026) noted that DWSIM's reactor models are equilibrium- or conversion-based rather than detailed chemical-kinetic solvers such as CHEMKIN. This distinction is particularly important for NO prediction because NO formation depends substantially on reaction kinetics rather than on equilibrium alone.

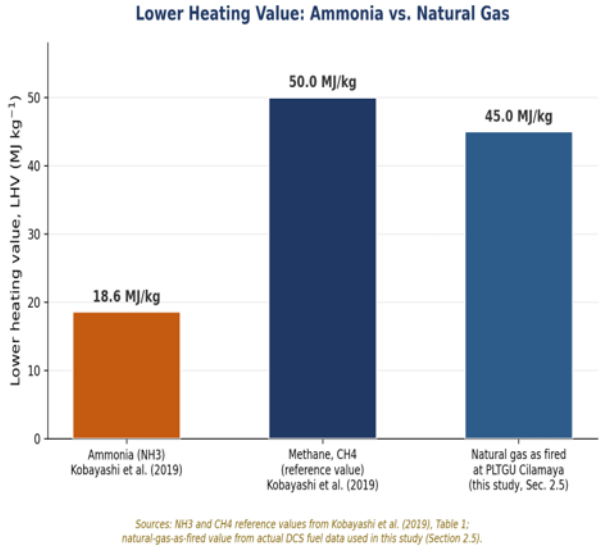



**Figure 5.** Lower heating value comparison. The original graphic retains 45 MJ/kg for natural gas; the reported simulation energy inputs instead imply 49.5 MJ/kg, which is used in the revised calculations.

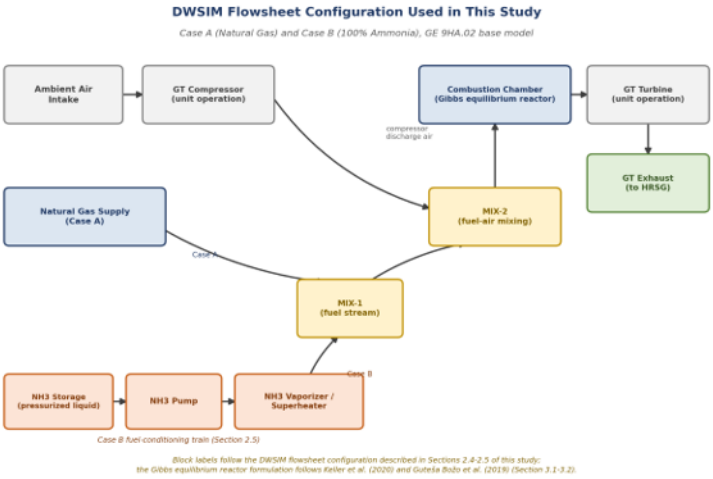



**Figure 6.** DWSIM schematic for natural gas and ammonia fuel paths. Its original heat-equivalence annotation is superseded by the revised 49.5 MJ/kg basis and Table 3.

**Process Simulation Platform**

Thermodynamic modeling was conducted in DWSIM, an open-source chemical process simulator. DWSIM was selected in light of the findings reported by Hassan & Manji (2023), who found that the platform could reproduce combined-cycle and gas turbine performance with deviations of well under 1% from actual plant data when properly calibrated. This precedent was relevant to the heavy-duty utility-scale gas turbine modeled in the present study. Because ammonia is a strongly polar, self-associating compound, the Peng–Robinson or Soave–Redlich–Kwong cubic equation of state was applied with explicit recognition of its limitations in predicting vapor–liquid equilibrium near ammonia's critical point (132.4 °C, 113.5 bar). These limitations were documented as modeling constraints rather than treated as evidence of unqualified predictive accuracy.

1. Base Model Development and Assessment (Case A: Natural Gas). The natural gas baseline model consisted of a compressor, a Gibbs equilibrium reactor, and a gas turbine configured using DCS-derived operating conditions for five load points. The prescribed inputs included air and fuel mass flow rates, supply conditions, and pressure ratios. Model performance was assessed by comparing simulated net power output with the corresponding DCS-recorded values. The resulting deviations were −20.20%, +3.01%, +6.82%, +6.94%, and +18.48% for Loads I–V, respectively. Only Load II satisfied the predefined 5% deviation criterion, indicating that the model did not demonstrate consistent agreement across all operating conditions. Consequently, the natural gas simulation was treated as a DCS-constrained baseline assessment rather than an independently validated model. The available manuscript did not establish a complete numerical calibration procedure or a consistent set of adjusted component-efficiency parameters. These limitations were considered when interpreting the subsequent ammonia-substitution results.
2. Fuel Substitution Scenario (Case B: 100% Ammonia). The reported Case B simulations replaced natural gas with pure ammonia at equal fuel mass flow rates under the load-associated air-side boundary conditions. This approach differed from one in which net power output was held constant. A separate heat-equivalence benchmark was calculated using the relationship (\dot{m}*{NG} \times 49.5 = \dot{m}*{NH_3} \times 18.6), with LHV expressed in MJ/kg. Table 3 presents the recalculated ammonia mass flow rates of 37.128, 42.432, 47.432, 51.765, and 63.794 kg/s. These values represented analytical estimates for equal heat input; they were not obtained from additional DWSIM runs and did not constitute verified equal-net-power operating points.

**Table 3**
*LHV-equivalent ammonia mass flow and proposed fuel-conditioning targets across Loads I–V.*

| Load | $NH_3$ mass flow (kg/s) | $NH_3$ supply pressure (bar-a) | $NH_3$ saturation temperature (°C) | Target heater outlet (°C) |
|---|---|---|---|---|
| I | 37.128 | 54.51 | 92.9 | ≥122.9 |
| II | 42.432 | 54.05 | 92.5 | ≥122.5 |
| III | 47.432 | 53.66 | 92.1 | ≥122.1 |
| IV | 51.765 | 53.41 | 91.9 | ≥121.9 |
| V | 63.794 | 52.83 | 91.4 | ≥121.4 |

Ammonia conditioning required separate consideration of phase behavior. At the reported header pressures of approximately 52.8–54.5 bar absolute, the source manuscript estimated saturation temperatures of 91–93 °C and proposed approximately 30 °C of superheat. These values were retained as provisional conditioning targets rather than validated equipment specifications. A pressurized liquid remains liquid until sufficient heating and vaporization occur; mixing alone does not necessarily cause it to enter a two-phase state. The proposed conditioning train comprised storage, pumping, and vaporization/superheating. Its thermal duty and the proposed outlet temperatures required verification using a documented ammonia property model before any claim of equal-net-power feasibility could be made.

3. Simulation Matrix and Parameters Analyzed. Combining five load points with two fuel cases yielded ten core DWSIM runs. This scope was deliberately chosen instead of a broader fuel-blend-ratio sweep so that each run could be examined in detail against its DCS-derived boundary conditions. Two groups of parameters were extracted from each run. The first group comprised thermodynamic performance parameters, including fuel mass flow, fuel heat input, combustion gas temperature, exhaust temperature, compressor power, turbine power, net power output, specific fuel consumption, and thermal efficiency. These parameters addressed RQ1 directly and, when compared across Loads I–V, supported the assessment of load-dependent performance differences associated with RQ2. The second group comprised emission parameters, including $CO_2$ mass flow, NO mass flow, and NO mole fraction. These parameters were estimated using a Gibbs free-energy equilibrium reactor and were evaluated alongside the thermodynamic performance parameters to address RQ3. Because DWSIM's equilibrium reactor estimated $NO_x$ formation from thermodynamic equilibrium rather than detailed chemical kinetics, absolute NO values were interpreted cautiously. They were discussed in relation to the kinetic-model and experimental findings synthesized in the preceding section rather than presented as stand-alone quantitative predictions.

**Data Analysis Approach**

For each load point, the Case A and Case B results were compared directly to address Research Question 1 (RQ1) by quantifying changes in each thermodynamic parameter when ammonia replaced natural gas at that load. Comparing these differences across Loads I–V addressed RQ2 by revealing whether the performance gap between the fuels widened, narrowed, or remained proportional as the load increased. The analysis also included calculations of ammonia mass flow rates corresponding to natural gas heat input or net power output at each load, while distinguishing analytical estimates from simulated operating points. Finally, $CO_2$ and NO results were examined alongside net power output and thermal efficiency for both fuel cases across all five loads to address RQ3. This comparison identified operating conditions under which emission reductions coincided with, or were offset by, changes in thermodynamic performance.

## RESULTS AND DISCUSSION

### Results

#### *Gas Turbine Operational Data*

Before presenting the comparative study of natural gas and ammonia simulation results in the following sections, this section reports the actual operating data recorded by the distributed control system (DCS) at PLTGU Cilamaya across five load conditions, designated Load I through Load V, that underpin the entire study. Table 4 reproduces this dataset in full, organized by physical subsystem: compressor, combustion chamber, and turbine. It includes all thirteen measured parameters used both to constrain the DWSIM baseline model described in the previous section and to establish the empirical baseline against which subsequent comparisons between natural gas and ammonia are made.

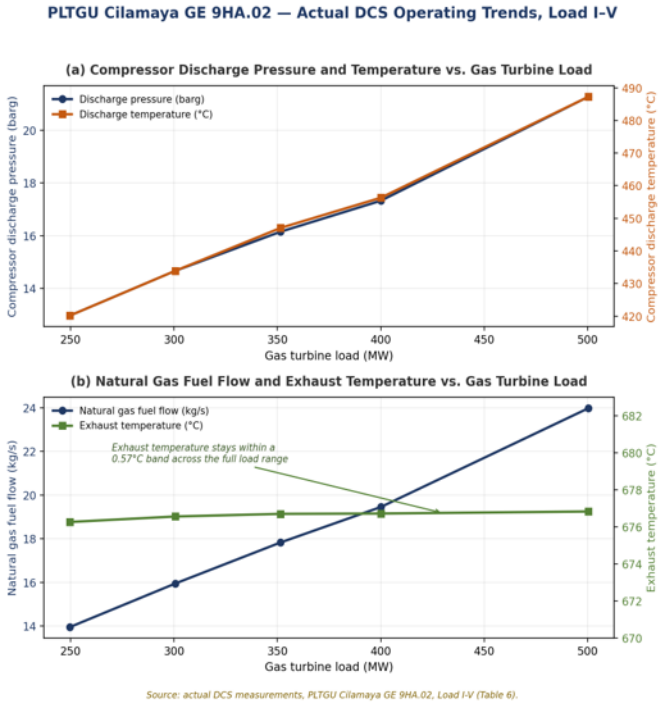



**Figure 7.** (a) Compressor discharge pressure and temperature vs. load; (b) fuel flow and exhaust temperature vs. load

**Table 4**

*Actual DCS-recorded operational data across Load I until load V*

| Parameter (Unit) | Load I | Load II | Load III | Load IV | Load V |
|---|---|---|---|---|---|
| Compressor | | | | | |
| Inlet air flow (kg/s) | 569.843 | 619.272 | 658.646 | 686.992 | 769.275 |
| Inlet air temperature (°C) | 24.321 | 24.163 | 24.200 | 25.053 | 24.922 |
| Relative humidity (%) | 90.889 | 91.471 | 91.145 | 86.873 | 89.506 |
| Ambient pressure (bara) | 1.008 | 1.007 | 1.007 | 1.008 | 1.005 |
| Discharge pressure (barg) | 12.968 | 14.665 | 16.150 | 17.329 | 21.273 |
| Pressure ratio (-) | 14.374 | 15.929 | 17.551 | 18.928 | 22.559 |
| Discharge temperature (°C) | 420.174 | 433.895 | 447.022 | 456.314 | 487.248 |
| Ambient temperature (°C) | 25.155 | 24.428 | 24.303 | 25.745 | 28.441 |
| Combustion Chamber | | | | | |
| Natural gas flow (kg/s) | 13.951 | 15.944 | 17.823 | 19.451 | 23.971 |
| Fuel temperature (°C) | 211.265 | 211.689 | 211.410 | 210.509 | 216.154 |
| Fuel supply pressure (barg) | 53.499 | 53.038 | 52.655 | 52.399 | 51.826 |
| Turbine | | | | | |

| | | | | | |
|---|---|---|---|---|---|
| Gas turbine load (MW) | 249.651 | 300.564 | 351.438 | 400.038 | 500.303 |
| Exhaust temperature, median (°C) | 676.268 | 676.564 | 676.706 | 676.723 | 676.835 |
| Exhaust mass flow (kg/s) | 621.502 | 678.349 | 735.841 | 787.831 | 930.127 |

The most notable trend in Table 4 concerns turbine exhaust temperature, which is presented alongside fuel flow rate in Figure 7(b). Although gas turbine load more than doubles, increasing from 249.651 MW at Load I to 500.303 MW at Load V, the median exhaust temperature varies by only 0.567°C, from 676.268°C at Load I to 676.835°C at Load V. This variation is much smaller than the corresponding 46–67°C increase in compressor discharge temperature over the same load range. This nearly invariant exhaust temperature is consistent with the temperature-control strategies employed in modern H-class gas turbines, such as the GE 9HA.02. These strategies may involve regulating inlet guide vane (IGV) position and, where applicable, adjusting combustion staging to maintain turbine inlet temperature and, consequently, exhaust temperature near the intended operating target across a wide load range. However, the precise control strategy depends on the turbine design and operating mode and should not be inferred from exhaust temperature alone. Maintaining suitable exhaust conditions can protect hot-section components from excessive thermal stress and, in a combined-cycle plant such as PLTGU Cilamaya, help preserve the thermal energy available to the downstream heat recovery steam generator (HRSG). By contrast, exhaust mass flow rate increases substantially with load, from 621.502 kg/s at Load I to 930.127 kg/s at Load V. This trend indicates that the increase in load is accompanied by a substantial increase in air and combustion-gas mass flow rather than a comparable increase in exhaust temperature.

The DCS dataset establishes the load-associated boundary conditions for the comparative study. When compressor inlet conditions, air composition, pressure ratio, and component settings are identical, compressor work should be the same in both fuel scenarios. Fuel substitution effects should therefore originate primarily in the combustion and expansion sections, subject to any differences in the specified operating conditions. The discrepancy in the reported Load III compressor results is addressed below. The equal-fuel-mass-flow comparison and the separate equal-energy-input benchmark represent different comparison bases. Neither should be interpreted as evidence of measured ammonia operation or verified equal-net-power substitution.

***Model simulation***

Figure 8 shows the DWSIM baseline flowsheet, comprising a compressor, a Gibbs reactor for combustion, and a turbine. The natural gas baseline uses DCS-recorded ambient conditions, fuel mass flow rate, and pressure ratio for the five operating loads. Simulated outputs are compared with available DCS measurements; prescribed inputs are not independent validation outputs. Percentage deviation and mean absolute percentage error (MAPE) are used to assess agreement, with 5% serving as an assessment threshold rather than proof of universal model validity. Hassan et al. (2026) provide a relevant precedent for DWSIM part-load modeling. The Peng–Robinson equation of state is used consistently throughout the present flowsheet, while Z. Liu & Karimi (2019) provide a related example of gas turbine process simulation.

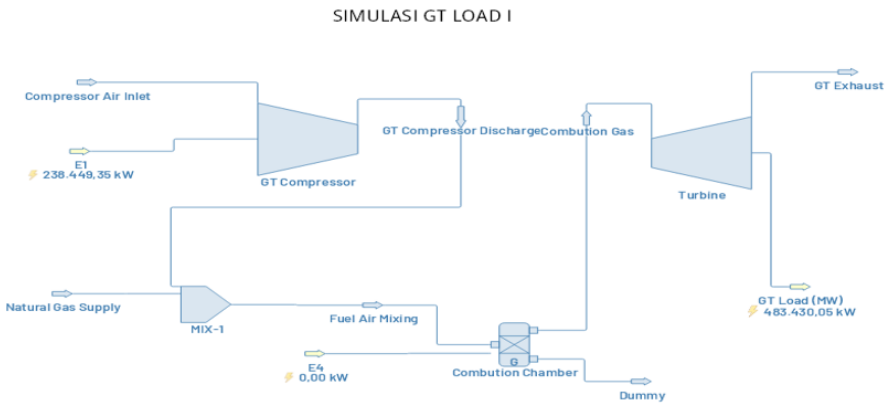



**Figure 8**. DWSIM baseline flowsheet for the natural-gas-fueled gas turbine.

## Discussion

### Comparative Thermodynamic Performance of Natural Gas and Ammonia at Five Actual Load Conditions

*Fuel Flow and Energy Input*

Figure 9 shows that fuel mass flow rate increases from 13.951 kg/s at Load I to 23.971 kg/s at Load V for both fuels, representing an increase of 71.82%. At equal fuel mass flow rates, ammonia supplies 37.58% of the thermal energy input supplied by natural gas: 259.489–445.861 MW compared with 690.575–1,186.565 MW, respectively. The corresponding energy-input deficit is 62.42%. These reported energy values imply lower heating values (LHVs) of 18.6 MJ/kg for ammonia and 49.5 MJ/kg for the simulated natural gas. (Kobayashi et al., 2019) report an LHV of 18.6 MJ/kg for ammonia and 50.0 MJ/kg for reference methane, corresponding to an energy-input ratio of 37.20%. The methane reference value must therefore be distinguished from the simulated natural gas value.

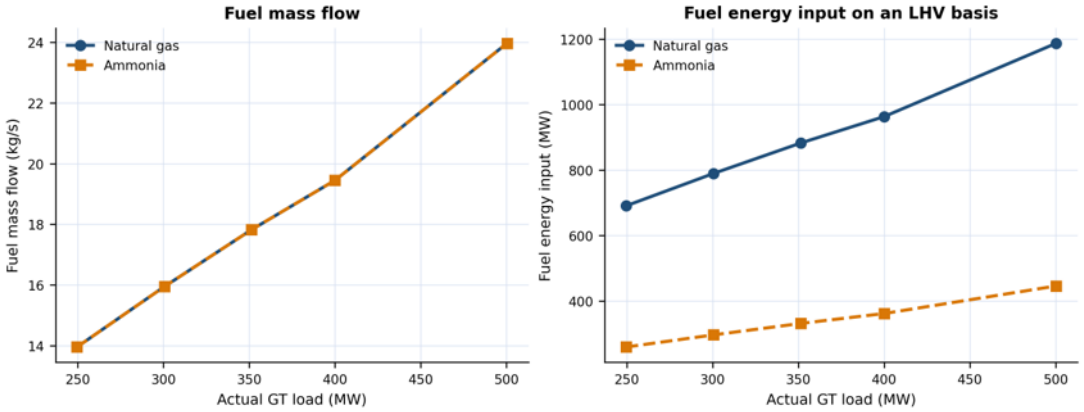



**Figure 9.** Trends in fuel mass flow and fuel energy input

*Combustion and Exhaust Temperatures*

The simulated reduction in combustion-gas temperature is consistent with the lower energy input associated with ammonia substitution at equal fuel mass flow rate. Report reference adiabatic flame temperatures of approximately 1,800°C for ammonia and 1,950°C for methane, together with maximum laminar burning velocities of 0.07 and 0.37 m/s, respectively (Kobayashi et al., 2019). However, these reference properties describe combustion characteristics under specified mixture conditions and are not directly equivalent to the combustor outlet temperatures obtained from the present DWSIM simulations. The substantially larger temperature reduction observed in the model, ranging from 41.50% to 42.36%, occurs under the imposed air-flow conditions and reduced ammonia energy input. Accordingly, the results should be interpreted as

consequences of the modeled operating boundaries rather than as direct measurements of ammonia flame behavior in an H-class gas turbine.

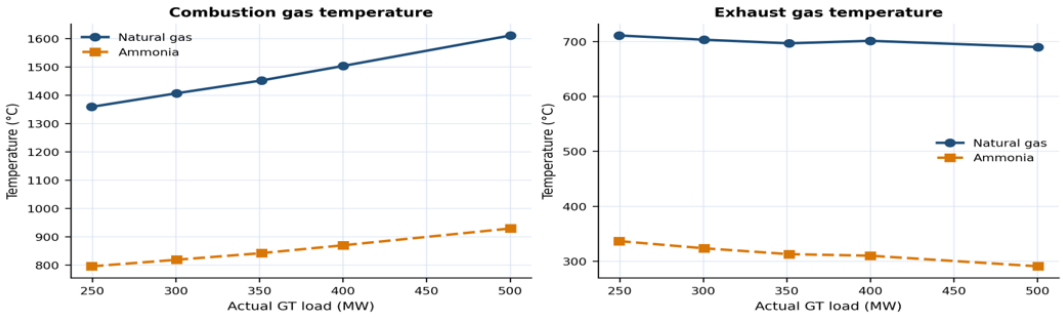



**Figure 10.** Trends in combustion gas and exhaust gas temperatures

*Compressor Work Turbine Work and Net Power*

Figure 11 compares compressor work, turbine work, and net power for natural gas and ammonia across the five operating conditions. Compressor work increases with the load-associated air-flow and pressure conditions, ranging from approximately 239.2 to 367.6 MW. Under identical compressor inlet conditions, air composition, pressure ratio, and isentropic efficiency, compressor work should remain unchanged between the two fuel scenarios. However, the reported Load III results show a discrepancy of 1.669 MW (0.59%). This difference cannot be attributed directly to fuel substitution and indicates an unresolved inconsistency in the simulation inputs, component settings, or reported results. Consequently, the Load III compressor-related performance comparison should be interpreted cautiously until the original simulation configuration has been verified. Across the reported operating conditions, ammonia produces lower turbine work and net power than natural gas at equal fuel mass flow rates, reflecting its substantially lower energy input under the simulated conditions.

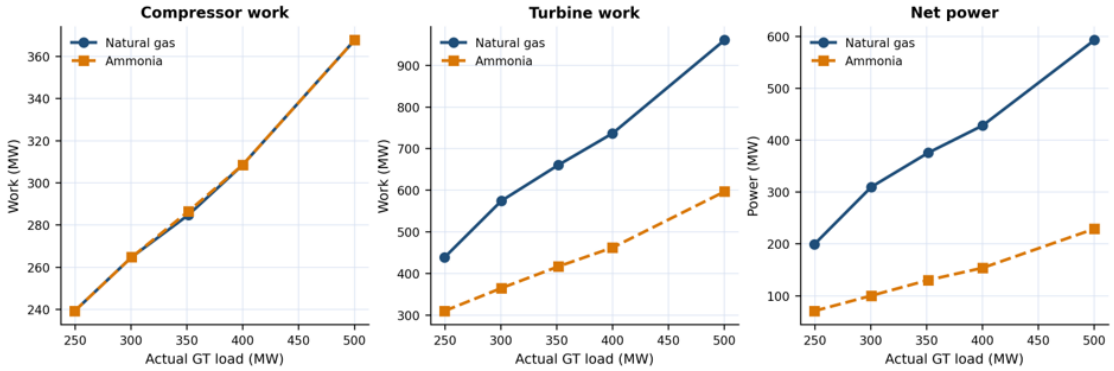



**Figure 11.** Trends in compressor work turbine work and net power

After subtracting compressor work from turbine work, the reported natural gas net power increases from 199.227 to 592.771 MW, while ammonia net power increases from 70.455 to 228.870 MW. Equal-mass-flow ammonia substitution therefore reduces net power by 61.39%–67.72%. The largest relative penalty occurs at Load II, where compressor work accounts for 72.59% of ammonia turbine work, compared with 46.09% for natural gas. In Figure 11, the natural gas result at Load V, 592.771 MW, is 21.771 MW, or 3.81%, above the GE 9HA.02 simple-cycle reference output of 571 MW (GE Vernova, 2020). This deviation may reflect differences between the manufacturer's reference rating and the present simulation, which uses measured operating inputs and an idealized DWSIM configuration. However, a valid comparison requires confirmation that both values represent the same power basis and that their operating conditions are comparable. By contrast, the ammonia gas turbine model reviewed by Pashchenko uses a reference net output of 40 MW and compressor and turbine isentropic efficiencies of 0.85 (Pashchenko, 2024). The present ammonia range of 70.455–228.870 MW is therefore 1.76–5.72 times that reference scale, highlighting the difference in scale between the present modeled

platform and the reference case.

***Thermal Efficiency and Overall Response to first Research question (RQ1)***

Natural gas thermal efficiency increases from 28.85% at Load I to 49.96% at Load V. Ammonia thermal efficiency increases from 27.15% to 51.33%. At Loads I–IV, ammonia efficiency is lower by 1.70, 5.53, 3.34, and 2.02 percentage points, respectively. This range is comparable to the 4-percentage-point reduction reported for a micro gas turbine operating with a 63% ammonia blend, for which efficiency decreased from 27% with methane to 23% with the ammonia blend. At Load V, ammonia efficiency exceeds natural gas efficiency by 1.38 percentage points. This crossover does not indicate equivalent power capability. Ammonia retains only 38.61% of natural gas net power at Load V because its energy input is also 62.42% lower. The apparent efficiency advantage reflects the ratio of net power to fuel energy input under the modeled conditions; it should not be attributed solely to the smaller denominator without examining the underlying turbine work and heat-transfer calculations.

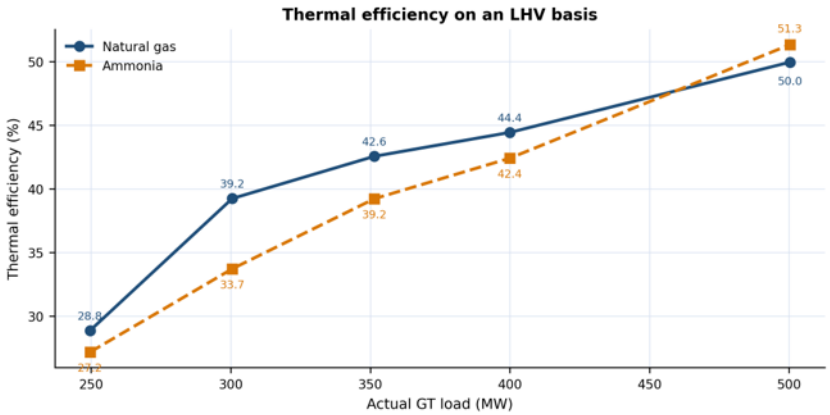



**Figure 12.** Trend in LHV based thermal efficiency

As an additional benchmark, the GE 9HA.02 datasheet reports a simple-cycle efficiency of 44.0% on an LHV basis and a net output of 571 MW under ISO conditions (GE Vernova, 2020). The Load IV natural gas efficiency of 44.43% differs from that reference by 0.43 percentage points, while the Load V value of 49.96% is 5.96 percentage points higher. The latter difference indicates that the model outputs should be interpreted as thermodynamic-cycle results rather than guaranteed plant performance. The literature also indicates that thermochemical ammonia recuperation can improve thermal efficiency by 5%–7%, while shifting the optimum pressure ratio from 11.8 to 10.3 at a turbine inlet temperature of 700°C and from 21.2 to 14.4 at 900°C (Pashchenko, 2024). These reported improvements suggest that heat recovery and partial ammonia decomposition are potential optimization strategies for reducing the power penalty observed in the present direct-combustion case.

In response to RQ1, replacing natural gas with ammonia at the same fuel mass flow rate leaves compressor work nearly unchanged but reduces fuel energy input by 62.42%, combustion-gas temperature by 41.50%–42.36%, exhaust-gas temperature by 52.69%–57.90%, turbine work by 29.37%–37.89%, and net power by 61.39%–67.72%. Thermal efficiency is lower by 1.70–5.53 percentage points at Loads I–IV and higher by 1.38 percentage points at Load V, although ammonia still supplies only 38.61% of natural gas net power at that load. Accordingly, pure ammonia is not a drop-in, equal-mass replacement when the performance target is equivalent output from an H-class gas turbine. Matching the natural gas output requires a higher ammonia mass flow rate, suitable combustor modifications, or an energy-recovery strategy such as thermochemical recuperation.

***Equivalent Ammonia Flow for Equal Gas Turbine Net Power***

RQ2 uses the simulated natural gas net power targets of 199.227, 309.623, 375.413, 427.819, and 592.771 MW. The ammonia regression fitted to five load-dependent points has a reported correlation coefficient of 0.99958 and an $R^2$ value of 0.99917. These statistics describe

the in-sample association. Air flow rate and pressure ratio also vary across the five points, so the fit cannot isolate the effect of fuel flow rate at a fixed load. Its inverse is used only for preliminary screening; fixed-boundary verification is required even for predictions within the sampled fuel-flow range. Using the residual definition of simulated natural gas net power minus DCS-recorded gas turbine load, the residuals at Loads I–V are −50.424, +9.059, +23.975, +27.781, and +92.468 MW. The MAPE is 11.09%, and the root mean square error (RMSE) is 50.04 MW. These baseline residuals are distinct from the residuals of the ammonia regression.

*Inverse Regression Method*

**Table 5**
*Predicted ammonia flow required to match natural gas net power*

| Condition | Actual load MW | Natural gas target net power MW | Natural gas flow kg/s | Equivalent ammonia flow kg/s | Ammonia flow increase % |
|---|---|---|---|---|---|
| Load I | 249.651 | 199.227 | 13.951 | 22.214 | 59.23 |
| Load II | 300.564 | 309.623 | 15.944 | 29.193 | 83.10 |
| Load III | 351.438 | 375.413 | 17.823 | 33.352 | 87.13 |
| Load IV | 400.038 | 427.819 | 19.451 | 36.665 | 88.50 |
| Load V | 500.303 | 592.771 | 23.971 | 47.093 | 96.46 |

The relationship between ammonia energy input and simulated net power was approximated using the reported linear regression equation, $W_{net,NH_3} = -152.177 + 0.85047\ Q_{NH_3}$, where net power and energy input are expressed in MW. By rearranging this equation and applying an ammonia LHV of 18.6 MJ/kg, preliminary ammonia mass-flow estimates were obtained for the natural gas net power targets presented in Table 5. The regression was fitted using five operating conditions in which air mass flow rate and pressure ratio varied simultaneously. Therefore, its coefficients cannot be interpreted as an isolated response to fuel flow rate under fixed operating conditions. The estimated ammonia flow rate for Load I lies within the original sampled flow range of 13.951–23.971 kg/s, whereas the estimates for Loads II–V exceed this range. These extrapolated values are useful for preliminary scenario screening but do not establish physically feasible equal-power operating conditions. Additional fixed-boundary DWSIM simulations, together with verification of combustion temperatures, equipment constraints, and emissions, are necessary before the estimated flow rates can be interpreted as operational requirements.

The inverse estimates span 22.214–47.093 kg/s, or 59.23%–96.46% above the corresponding natural gas flow rates. The Load I estimate lies within the sampled flow interval, although its boundary conditions differ from those of the other training points. The estimates for Loads II–V exceed the sampled maximum and are therefore extrapolations. The equal-energy-input benchmark, calculated using an LHV of 49.5 MJ/kg for natural gas and 18.6 MJ/kg for ammonia, is 37.128–63.794 kg/s. Neither benchmark establishes a verified operating requirement. Fixed-load DWSIM calculations must assess fuel flow rate, temperature limits, and emissions together.

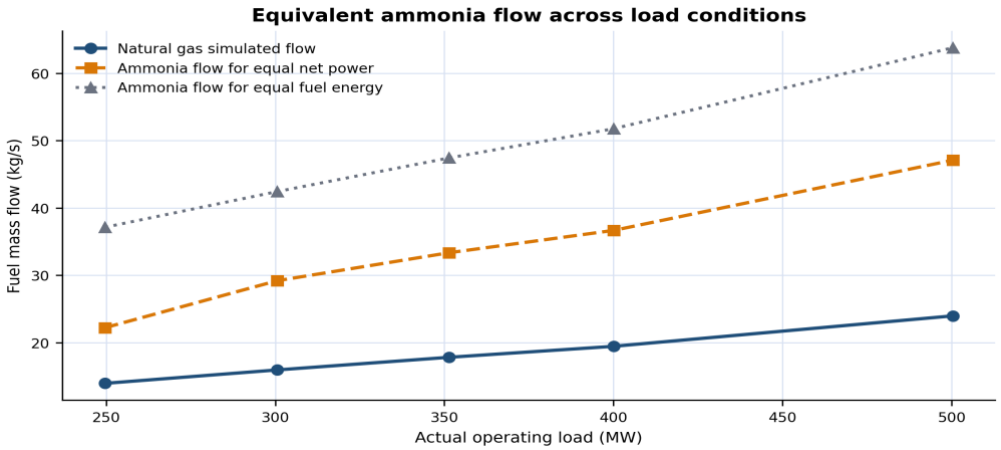



**Figure 13.** Natural gas flow predicted equal power ammonia flow and equal energy ammonia benchmark

The inverse fit yields ammonia energy inputs of approximately 413.188–875.925 MW. These algebraic estimates remain 26.18%–40.17% below the reported natural gas energy inputs. This apparent advantage cannot be interpreted as verified conversion performance because the regression combines changing air-side operating conditions and extends beyond the sampled ammonia flow range. It therefore provides candidate starting points for new fixed-boundary simulations rather than evidence of improved real-engine efficiency.

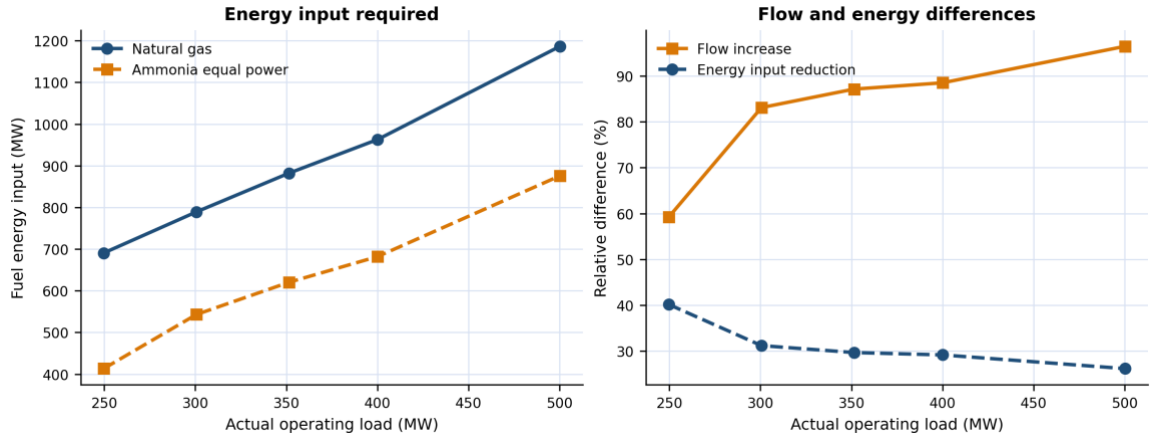



**Figure 14**. Comparison of fuel energy input and percentage differences for preliminary equal-net-power ammonia flow estimates.

*Performance Gap Before Flow Adjustment*

At the original equal-mass-flow condition, ammonia produces only 70.455–228.870 MW, compared with 199.227–592.771 MW for natural gas. The corresponding initial net power deficit ranges from 61.39% to 67.72%. Its absolute magnitude increases from 128.772 MW at Load I to 363.901 MW at Load V. Consequently, increasing load amplifies the absolute power shortfall, even though the relative deficit becomes less severe at the highest load. Flow adjustment is therefore essential when equal power, rather than equal fuel mass, is the comparison criterion.

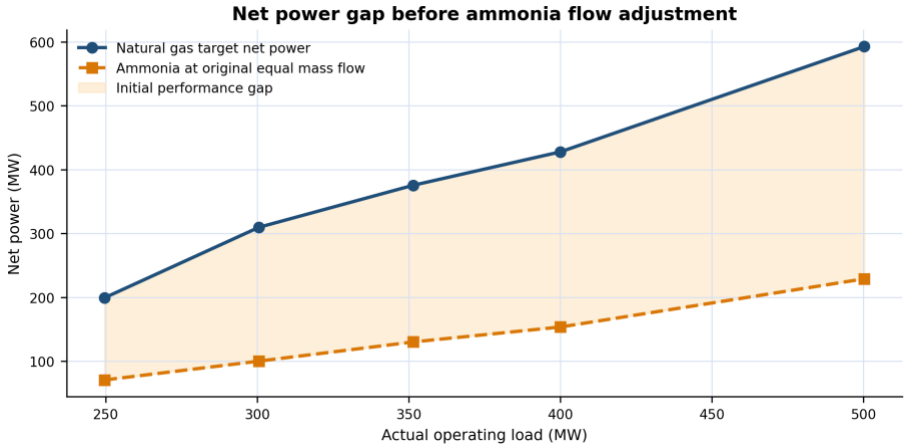



**Figure 15**. Net power difference before equivalent ammonia flow adjustment

*Optimization Objective and Operating Constraints*

The inverse regression provides an initial estimate of ammonia flow rate, while the final operating point should be selected through constrained optimization. The primary objective is to minimize ammonia mass flow rate while matching the target net power. Feasibility also requires turbine inlet temperature, exhaust temperature, nitrogen oxide emissions, and unburned ammonia slip to remain within their allowable limits. If multiple feasible solutions exist, a weighted objective function can combine power mismatch, specific ammonia consumption, nitrogen oxide emissions, and ammonia slip. The feasible condition with the lowest objective-function value is then selected as the preferred operating point.

$$\min \dot{m}_{NH_3}$$
$$W_{net,\,NH_3} = W_{target}$$
$$TIT_{NH_3} \leq TIT_{limit}$$
$$T_{exhaust,\,NH_3} \leq T_{exhaust,\,limit}$$
$$NO_x \leq NO_{x,\,limit}$$
$$NH_3\ slip \leq NH_{3,\,limit}$$

$$J = w_1 \left| \frac{W_{net} - W_{target}}{W_{target}} \right| + w_2 \frac{\dot{m}_{NH_3}}{W_{net}} + w_3 \frac{NO_x}{NO_{x,\,limit}} + w_4 \frac{NH_3\ slip}{NH_{3,\,limit}}$$

Minimum J defines the preferred feasible operating condition.

**Figure 16**. Proposed objective function and constraints for ammonia flow optimization

Numerical constraint verification cannot be completed using the present regression alone because turbine inlet temperature, nitrogen oxide concentration, and ammonia slip were not recalculated at the predicted equivalent flow rates. Each predicted point must therefore be evaluated using the DWSIM model. A practical search procedure is to increase ammonia flow rate from the values in Table 5 in small increments, solve the reactor and turbine models, retain only the cases that satisfy all constraints, and select the feasible point with the lowest objective-function value. Pashchenko (2024) reports that thermochemical ammonia recuperation can improve efficiency by 5%–7% and lower the optimum pressure ratio from 21.2 to 14.4 at a turbine inlet temperature of 900°C. These findings support investigating heat recovery and pressure-ratio optimization when direct ammonia flow adjustment alone violates thermal or emissions constraints.

Based on inverse regression, the preliminary ammonia flow rates estimated to reproduce natural gas net power are 22.214, 29.193, 33.352, 36.665, and 47.093 kg/s for Loads I–V, respectively. These values are 59.23%–96.46% greater than the corresponding natural gas flow rates. Higher loads require both higher ammonia mass flow rates and greater energy input, while the predicted relative energy-input gap between ammonia and natural gas narrows from 40.17% to 26.18%. Before flow correction, ammonia net power is 61.39%–67.72% lower than natural gas net power. These estimates address the comparative component of RQ2, but values above 23.971

kg/s remain extrapolations and require direct simulation verification against temperature, nitrogen oxide, and ammonia-slip constraints.

***Performance and Emission Trade Off of Natural Gas and Ammonia***

This section addresses RQ3 by evaluating the trade-off between thermodynamic performance and equilibrium predictions of carbon dioxide and nitric oxide at five actual H-class gas turbine operating conditions. Absolute emission mass flow rates indicate total pollutant production, whereas emission intensity expresses pollutant mass per unit of net electricity generated. Both measures are necessary because load affects fuel consumption and power output simultaneously. The assessment uses the equal-fuel-mass-flow simulations from the preceding section rather than the extrapolated equal-power ammonia flow rates.

*Thermodynamic Performance across Load*

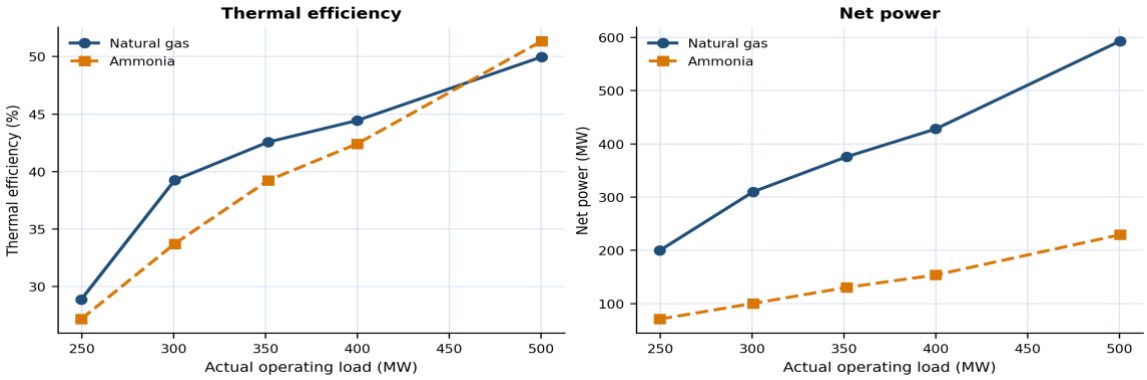



**Figure 17.** Trends in thermal efficiency and net power

Figure 17 shows that natural gas net power increases from 199.227 to 592.771 MW, whereas ammonia net power increases from 70.455 to 228.870 MW. At the same fuel mass flow rate, ammonia retains only 32.28%–38.61% of natural gas net power. Thermal efficiency improves with load for both fuels. Natural gas efficiency increases from 28.85% to 49.96%, while ammonia efficiency increases from 27.15% to 51.33%. The higher ammonia efficiency at Load V does not eliminate the output penalty because its chemical energy input is substantially lower. Performance evaluation must therefore consider thermal efficiency and delivered power together.

*Carbon Dioxide and Nitric Oxide Predictions*

Natural gas $CO_2$ mass flow rate increases from 38.3892 to 65.9550 kg/s. Pure ammonia produces zero fuel-derived $CO_2$ in the model because it contains no carbon; emissions associated with upstream production, transport, and conditioning are excluded. Natural gas NO mass flow rate increases from 1.07785 to 3.17484 kg/s, compared with 0.03922–0.16161 kg/s for ammonia. The endpoint comparisons correspond to 96.36% and 94.91% lower NO mass flow rates, respectively. These results are thermodynamic-equilibrium predictions obtained at different combustion temperatures, not demonstrated reductions in actual fuel-NO formation or total $NO_x$ emissions. Kinetic modeling and experimental verification are required.

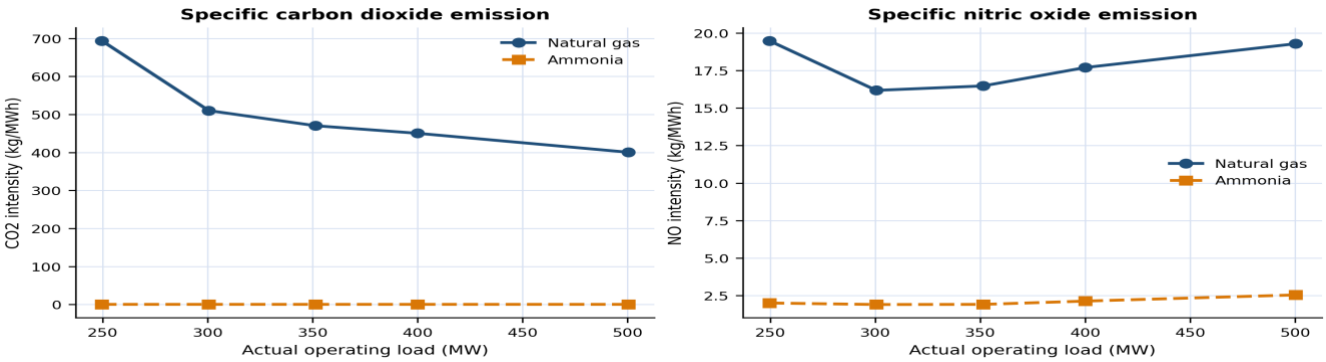



**Figure 18**. Trends in specific carbon dioxide and nitric oxide emissions

Emission intensity provides a more useful comparison across loads than mass flow rate alone. Natural gas $CO_2$ intensity decreases continuously from 693.68 to 400.58 kg/MWh as thermal efficiency and net output increase. Natural gas NO intensity reaches its minimum of 16.17 kg/MWh at Load II, then increases to 19.28 kg/MWh at Load V. Ammonia $CO_2$ intensity remains zero, while ammonia NO intensity is lowest at Load II, at 1.903 kg/MWh; remains nearly unchanged at Load III, at 1.912 kg/MWh; and increases to 2.542 kg/MWh at Load V. Thus, higher loads favor carbon efficiency but impose a NO-related penalty in the equilibrium results.

*Quantitative Trade Off and Preferred Load*

A normalized performance–emission index was used to compare the five operating conditions based on thermal efficiency, $CO_2$ emission intensity, and NO emission intensity. The respective weighting factors were 40%, 30%, and 30%. Each indicator was normalized across the evaluated operating conditions, with the most favorable value assigned the highest score and the least favorable value assigned the lowest score. Because the modeled ammonia scenario produces zero direct fuel-derived $CO_2$ at every load, its $CO_2$ component contributes equally across all evaluated conditions. The combined index represents the arithmetic mean of the natural gas and ammonia scores. These weighting factors are analytical assumptions introduced for comparative assessment and do not represent regulatory thresholds or experimentally established operating priorities. Consequently, the resulting ranking identifies the preferred condition only within the specified normalization method, weighting structure, and equal-fuel-mass-flow simulation scenarios.

Load III achieves the highest combined score of 77.84, followed by Load IV at 72.58 and Load V at 70.89. Load III is selected as the preferred compromise because it provides natural gas and ammonia efficiencies of 42.55% and 39.21%, respectively, while NO intensities remain near their minimum values, at 16.47 kg/MWh for natural gas and 1.912 kg/MWh for ammonia. Load V delivers the highest efficiencies, but its NO intensities increase to 19.28 and 2.542 kg/MWh, respectively. Load II minimizes NO intensity, although its lower efficiencies reduce its overall balance score.

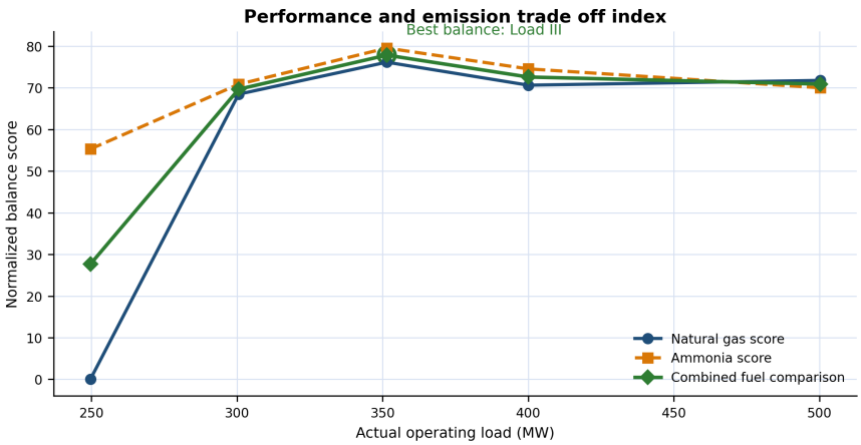



**Figure 19.** Normalized performance and emission trade off index

Published results for ammonia combustion span a wide range because emissions depend on equivalence ratio, pressure, residence time, mixing, combustion staging, and heat loss. Pashchenko (2024) reviews ammonia gas turbine development and fuel-processing strategies. Saif & Mokheimer (2025) discuss emissions control through combustor design and fuel blending. These studies support a qualitative comparison with the present equilibrium results. Concentrations reported in parts per million (ppm) cannot be compared directly with mass flow rates in kg/s or emission intensities in kg/MWh without consistent exhaust-flow and oxygen-correction definitions. Literature values obtained under different conditions are therefore not treated as quantitative validation of the present model.

The present model reports pollutant mass flow rates rather than dry, oxygen-corrected concentrations. Its results cannot therefore be directly compared with published ppm values without information on exhaust molar flow rate, oxygen correction, pressure, and temperature. More importantly, a Gibbs reactor determines equilibrium composition but does not reproduce finite reaction rates, flame stabilization, local temperature gradients, residence time, staged mixing, nitrogen dioxide ($NO_2$), nitrous oxide ($N_2O$), or unburned ammonia slip. The predicted ammonia NO advantage should therefore be interpreted as an equilibrium tendency, not as evidence that a real ammonia combustor will emit less NO than a natural gas combustor.

Natural gas provides substantially higher net power at equal fuel mass flow rate, but its direct $CO_2$ emissions increase from 38.3892 to 65.9550 kg/s. Ammonia eliminates direct fuel-derived $CO_2$ within the model boundary and predicts 94.91%–96.36% lower NO mass flow rates, although it retains only 32.28%–38.61% of natural gas net power. Increasing load improves thermal efficiency and reduces natural gas $CO_2$ intensity, but it raises absolute NO flow and eventually increases NO intensity. Under the specified weighting of 40% for efficiency, 30% for $CO_2$ intensity, and 30% for NO intensity, Load III provides the best overall balance. Load V is preferred when maximum efficiency and power are the primary objectives, whereas Load II is preferred when minimizing NO intensity is the main criterion. The Load III conclusion applies only to the present equilibrium model and must be verified using kinetic combustion analysis and corrected exhaust concentration data.

## CONCLUSION

The comparative DWSIM simulations across five DCS-derived operating conditions demonstrate substantial differences between natural gas and ammonia as fuels for an H-class gas turbine. At equal fuel mass flow rates, natural gas generates 199.227–592.771 MW of net power, whereas ammonia produces 70.455–228.870 MW, reflecting the lower energy input associated with ammonia substitution. Although ammonia achieves higher simulated thermal efficiency at Load V, this result does not compensate for its substantially lower net power. Preliminary inverse regression estimates that ammonia mass flow rates of 22.214–47.093 kg/s would be required to match the simulated natural gas power targets, representing increases of 59.23%–96.46% relative to the corresponding natural gas flow rates. However, these estimates were derived from load-dependent operating conditions and should not be interpreted as verified equal-power operating points without additional fixed-boundary simulations.

Regarding environmental performance, pure ammonia produces zero direct fuel-derived $CO_2$ within the modeled combustion boundary, while its predicted equilibrium NO mass flow rate is 94.91%–96.36% lower than that of natural gas at the evaluated endpoint conditions. These results are equilibrium-model predictions rather than experimentally demonstrated reductions in actual gas turbine emissions. Under the specified performance–emission weighting criteria, Load III achieves the highest combined assessment score, although this preference remains conditional on the selected indicators and simulation assumptions. The principal limitations include discrepancies between simulated and recorded baseline power, incomplete calibration documentation, simplified equilibrium chemistry, and extrapolation of ammonia fuel requirements. Future investigations should prioritize independent model validation, combustion-kinetic analysis, verification of ammonia conditioning requirements and equipment constraints, assessment of ammonia slip, and evaluation of life-cycle environmental and economic implications before practical implementation is considered.

**ACKNOWLEDGEMENT**

The authors acknowledge the Master Program of Energy, Diponegoro University, and PLTGU Cilamaya for academic support and access to operational data.

**AUTHOR CONTRIBUTION STATEMENT**

Conceptualization, methodology, and original draft preparation, Dapot Boni Tua Rajagukguk; supervision and revisi, S. Silviana and M. Muchammad. All authors have read and approved the manuscript.

**REFERENCES**

Çengel, Y. a. (2004). Thermodynamics: An Engineering Approach. *McGraw-Hill*.

Fawwaz Aalrebei, O., Hamdan Al Assaf, A., Amhamed, A., Swaminathan, N., & Hewlett, S. (2022). Ammonia-hydrogen-air gas turbine cycle and control analyses. *International Journal of Hydrogen Energy*, *47*(13), 8603–8620. https://doi.org/10.1016/j.ijhydene.2021.12.190

GE Vernova. (2020). 9HA gas turbine (Datasheet GEA32927A). https://www.gevernova.com/gas-power/products/gas-turbines/9ha

Guteša Božo, M., Vigueras-Zuniga, MO., Buffi, M., Seljak, T., & Valera-Medina, A. (2019). Fuel rich ammonia-hydrogen injection for humidified gas turbines. *Applied Energy*, *251*, 113334. https://doi.org/10.1016/j.apenergy.2019.113334

Hassan, T. N., & Manji, S. T. (2023). Simulating Combined Cycle and Gas Turbine Power Plant under Design Condition using Open-Source Software DWSIM. *ARO-THE SCIENTIFIC JOURNAL OF KOYA UNIVERSITY*, *11*(1), 60–71. https://doi.org/10.14500/aro.11098

Hassan, T. N., Manji, S. T., & Maaroof, A. A. (2026). Part-Load Simulation of Combined Cycle and Gas Turbine Power Plants Using DWSIM. *ARO-THE SCIENTIFIC JOURNAL OF KOYA UNIVERSITY*, *14*(1), 337–348. https://doi.org/10.14500/aro.12620

Kang, L., Pan, W., Zhang, J., Wang, W., & Tang, C. (2023). A review on ammonia blends combustion for industrial applications. *Fuel*, *332*, 126150. https://doi.org/10.1016/j.fuel.2022.126150

Keller, M., Koshi, M., Otomo, J., Iwasaki, H., Mitsumori, T., & Yamada, K. (2020). Thermodynamic evaluation of an ammonia-fueled combined-cycle gas turbine process operated under fuel-rich conditions. *Energy*, *194*, 116894. https://doi.org/10.1016/j.energy.2020.116894

Kobayashi, H., Hayakawa, A., Somarathne, K. D. K. A., & Okafor, E. C. (2019). Science and technology of ammonia combustion. *Proceedings of the Combustion Institute*, *37*(1), 109–133. https://doi.org/10.1016/j.proci.2018.09.029

Kurata, O., Iki, N., Matsunuma, T., Inoue, T., Tsujimura, T., Furutani, H., Kobayashi, H., & Hayakawa, A. (2017). Performances and emission characteristics of NH3–air and NH3CH4–air combustion gas-turbine power generations. *Proceedings of the Combustion Institute*, *36*(3), 3351–3359. https://doi.org/10.1016/j.proci.2016.07.088

Kurata, O., Iki, N., Matsunuma, T., Maeda, T., Hirano, S., Kadoguchi, K., Takeuchi, H., & Yoshida, H. (2014). Micro gas turbine cogeneration system with latent heat storage at the University: Part II: Part load and thermal priority mode. *Applied Thermal Engineering*, *65*(1–2), 246–254. https://doi.org/10.1016/j.applthermaleng.2013.12.050

Liu, L., Wu, Y., Wang, Y., Wu, J., & Fu, S. (2022). Exploration of environmentally friendly marine power technology -ammonia/diesel stratified injection. *Journal of Cleaner Production*, *380*, 135014. https://doi.org/10.1016/j.jclepro.2022.135014

Liu, Z., & Karimi, I. A. (2019). Simulation of a combined cycle gas turbine power plant in Aspen HYSYS. *Energy Procedia*, *158*, 3620–3625. https://doi.org/10.1016/j.egypro.2019.01.901

Okafor, E. C., Somarathne, K. D. K. A., Hayakawa, A., Kudo, T., Kurata, O., Iki, N., & Kobayashi, H. (2019). Towards the development of an efficient low-NOx ammonia combustor for a micro gas turbine. *Proceedings of the Combustion Institute*, *37*(4), 4597–4606. https://doi.org/10.1016/j.proci.2018.07.083

Pashchenko, D. (2023). Hydrogen-rich gas as a fuel for the gas turbines: A pathway to lower CO2 emission. *Renewable and Sustainable Energy Reviews*, *173*, 113117. https://doi.org/10.1016/j.rser.2022.113117

Pashchenko, D. (2024). Ammonia fired gas turbines: Recent advances and future perspectives. *Energy*, *290*, 130275. https://doi.org/10.1016/j.energy.2024.130275

Saif, A. G. H., & Mokheimer, E. M. A. (2025). Comprehensive review on ammonia combustion technologies: Combustion characteristics, potential of hydrogen/methane additions, and emerging applications. *International Journal of Hydrogen Energy*, *148*, 149672. https://doi.org/10.1016/j.ijhydene.2025.05.302

Somarathne, K. D. K. A., Hatakeyama, S., Hayakawa, A., & Kobayashi, H. (2017). Numerical study of a low emission gas turbine like combustor for turbulent ammonia/air premixed swirl flames with a secondary air injection at high pressure. *International Journal of Hydrogen Energy*, *42*(44), 27388–27399. https://doi.org/10.1016/j.ijhydene.2017.09.089

Valera-Medina, A., Xiao, H., Owen-Jones, M., David, W. I. F., & Bowen, P. J. (2018). Ammonia for power. *Progress in Energy and Combustion Science*, *69*, 63–102. https://doi.org/10.1016/j.pecs.2018.07.001

Xiao, H., Valera-Medina, A., & Bowen, P. J. (2017). Study on premixed combustion characteristics of co-firing ammonia/methane fuels. *Energy*, *140*, 125–135. https://doi.org/10.1016/j.energy.2017.08.077